

Journal Pre-proof

Unravelling host-pathogen interactions by biofilm infected human wound models

Jana Wächter, Pia K. Vestweber, Viktoria Planz, Maike Windbergs



PII: S2590-2075(23)00061-8

DOI: <https://doi.org/10.1016/j.biofilm.2023.100164>

Reference: BIOFLM 100164

To appear in: *Biofilm*

Received Date: 22 September 2023

Revised Date: 19 October 2023

Accepted Date: 20 October 2023

Please cite this article as: Wächter J, Vestweber PK, Planz V, Windbergs M, Unravelling host-pathogen interactions by biofilm infected human wound models, *Biofilm* (2023), doi: <https://doi.org/10.1016/j.biofilm.2023.100164>.

This is a PDF file of an article that has undergone enhancements after acceptance, such as the addition of a cover page and metadata, and formatting for readability, but it is not yet the definitive version of record. This version will undergo additional copyediting, typesetting and review before it is published in its final form, but we are providing this version to give early visibility of the article. Please note that, during the production process, errors may be discovered which could affect the content, and all legal disclaimers that apply to the journal pertain.

© 2023 Published by Elsevier B.V.

Credit Author Statement

Jana Wächter: Methodology, validation, investigation, formal analysis, writing – original draft, writing – review and editing, visualization

Pia K Vestweber: Methodology, validation, investigation, formal analysis, writing – original draft, writing – review and editing, visualization

Viktorija Planz: Methodology, validation, writing – original draft, writing – review and editing

Maike Windbergs: Conceptualization, resources, writing – original draft, writing – review and editing, supervision, project administration, funding acquisition

Journal Pre-proof

Unravelling host-pathogen interactions by biofilm infected human wound models

Jana Wächter^{1#}, Pia K Vestweber^{1#}, Viktoria Planz¹ and Maike Windbergs¹

¹Institute of Pharmaceutical Technology and Buchmann Institute for Molecular Life Sciences, Goethe University Frankfurt, Frankfurt am Main, Germany

#These authors contributed equally to this work.

Abstract

Approximately 80% of persistent wound infections are affected by the presence of bacterial biofilms, resulting in a severe clinical challenge associated with prolonged healing periods, increased morbidity, and high healthcare costs. Unfortunately, *in vitro* models for wound infection research almost exclusively focus on early infection stages with planktonic bacteria. In this study, we present a new approach to emulate biofilm-infected human wounds by three-dimensional human *in vitro* systems. For this purpose, a matured biofilm consisting of the clinical key wound pathogen *Pseudomonas aeruginosa* was pre-cultivated on electrospun scaffolds allowing for non-destructive transfer of the matured biofilm to human *in vitro* wound models. We infected tissue-engineered human *in vitro* skin models as well as *ex vivo* human skin explants with the biofilm and analyzed structural tissue characteristics, biofilm growth behavior, and biofilm-tissue interactions. The structural development of biofilms in close proximity to the tissue, resulting in high bacterial burden and *in vivo*-like morphology, confirmed a manifest wound infection on all tested wound models, validating their applicability for general investigations of biofilm growth and structure. The extent of bacterial colonization of the wound bed, as well as the subsequent changes in molecular composition of skin tissue, were inherently linked to the characteristics of the underlying wound models including their viability and origin. Notably, the immune response observed in viable *ex vivo* and *in vitro* models was consistent with previous *in vivo* reports. While *ex vivo* models offered greater complexity and closer similarity to the *in vivo* conditions, *in vitro* models consistently demonstrated higher reproducibility. As a consequence, when focusing on direct biofilm-skin interactions, the viability of the wound models as well as their advantages and limitations should be aligned to the particular research question of future studies. Altogether, the novel model allows for a systematic investigation of host-pathogen interactions of bacterial biofilms and human wound tissue, also paving the way for development and predictive testing of novel therapeutics to combat biofilm-infected wounds.

Keywords

bacterial biofilms, *in vitro* skin infection model, host-biofilm interactions, persistent wound infections, innate immune response

Correspondence address:

Prof. Dr. Maike Windbergs, Institute of Pharmaceutical Technology and Buchmann Institute for Molecular Life Sciences, Goethe University Frankfurt, Max-von-Laue-Str. 9, 60438 Frankfurt am Main, Germany, E-Mail: windbergs@em.uni-frankfurt.de

1 **Unravelling host-pathogen interactions by biofilm infected human wound** 2 **models**

3 **Abstract**

4 Approximately 80% of persistent wound infections are affected by the presence of bacterial biofilms, resulting
5 in a severe clinical challenge associated with prolonged healing periods, increased morbidity, and high healthcare
6 costs. Unfortunately, *in vitro* models for wound infection research almost exclusively focus on early infection
7 stages with planktonic bacteria. In this study, we present a new approach to emulate biofilm-infected human
8 wounds by three-dimensional human *in vitro* systems. For this purpose, a matured biofilm consisting of the
9 clinical key wound pathogen *Pseudomonas aeruginosa* was pre-cultivated on electrospun scaffolds allowing for
10 non-destructive transfer of the matured biofilm to human *in vitro* wound models. We infected tissue-engineered
11 human *in vitro* skin models as well as *ex vivo* human skin explants with the biofilm and analyzed structural tissue
12 characteristics, biofilm growth behavior, and biofilm-tissue interactions. The structural development of biofilms
13 in close proximity to the tissue, resulting in high bacterial burden and *in vivo*-like morphology, confirmed a
14 manifest wound infection on all tested wound models, validating their applicability for general investigations of
15 biofilm growth and structure. The extent of bacterial colonization of the wound bed, as well as the subsequent
16 changes in molecular composition of skin tissue, were inherently linked to the characteristics of the underlying
17 wound models including their viability and origin. Notably, the immune response observed in viable *ex vivo* and
18 *in vitro* models was consistent with previous *in vivo* reports. While *ex vivo* models offered greater complexity and
19 closer similarity to the *in vivo* conditions, *in vitro* models consistently demonstrated higher reproducibility. As a
20 consequence, when focusing on direct biofilm-skin interactions, the viability of the wound models as well as their
21 advantages and limitations should be aligned to the particular research question of future studies. Altogether,
22 the novel model allows for a systematic investigation of host-pathogen interactions of bacterial biofilms and
23 human wound tissue, also paving the way for development and predictive testing of novel therapeutics to
24 combat biofilm-infected wounds.

25 **Keywords**

26 bacterial biofilms, *in vitro* skin infection model, host-biofilm interactions, persistent wound infections, innate
27 immune response

28

29 Introduction

30 Impaired wound healing represents a major burden for today's healthcare system, as it not only significantly
31 decreases the patients' quality of life but also has a high socio-economic impact [1]. Even worse, approximately
32 80% of such wounds are affected by bacterial biofilms according to a meta-analysis of clinical studies [2]. Bacterial
33 biofilms are characterized as persistent, structurally organized clusters of bacteria in a matrix, forming a
34 protective shield against the host's immune defense mechanisms and fostering antimicrobial resistance [3].
35 Biofilm models cultivated *in vitro* on artificial surfaces have successfully been used to gain a molecular and
36 mechanistic understanding of biofilm formation and maturation [4]. However, to understand interactions of
37 biofilm and biological tissue for the development and testing of effective therapeutics against wound infections,
38 both components, the biofilm and the tissue, need to be represented in a suitable model.

39 *In vivo* animal models are frequently used, with mice being the predominant species, accounting for over 70% of
40 the total usage in Germany [5,6]. However, particularly in wound infection studies, the translatability of murine
41 models to the human *in vivo* situation is limited due to differences in immune response and anatomy of the skin
42 itself [7,8]. Further, the contraction of mouse skin upon wounding caused by an additional muscle layer in rodent
43 skin (*panniculus carnosus*) poses another problem. Additional major disadvantages comprise high costs and
44 lacking standardization of experimental set-ups [9,10]. Against this background, the development of alternative
45 human-based biofilm-infected wound models is of particular importance.

46 In general, *in vitro* wound models range from two-dimensional cell monolayers over three-dimensional
47 tissue-engineered human skin models to human skin explants (*ex vivo* models) [11,12]. While cell monolayers
48 offer a simple method for basic research purposes, the pathophysiology and microenvironment of human skin
49 *in vivo* is not accurately reflected, since bacterial invasion and interaction with different cell types or the
50 extracellular matrix cannot be mimicked [13]. Three dimensional models containing all layers of the native
51 epidermis and dermis represent a more sophisticated approach. Briefly, they are generated by culturing dermal
52 fibroblasts in a matrix in combination with primary keratinocytes at the air-liquid interface. Several providers
53 offer commercially available human skin models, allowing for standardization across different laboratories [13].
54 Still, other features of the skin including immune cells or hair follicles are usually missing. Full human skin explants
55 depict more native conditions, as they include all cellular elements and their interactions [9].

56 Different approaches for mimicking infected wounds with bacterial biofilms *in vitro*, either with tissue-
57 engineered human *in vitro* skin models or *ex vivo* human skin biopsies, are reported in literature [14–16]. The
58 co-cultivation of such *in vitro* human skin tissue models with bacteria is generally challenging, as cultivation
59 media provide an excessive nutrition source for bacteria further promoting their exponential replication kinetics.
60 This results in overgrowth of the skin tissue by bacteria as well as toxic effects on the cells, significantly reducing
61 their viability [17]. As a bacterial biofilm requires up to several days for maturation, direct inoculation of skin
62 tissue with bacteria and subsequent biofilm formation and maturation in direct co-culture (as performed in
63 animal models) is impossible [18]. Nevertheless, this method is still used in *in vitro* studies for extremely limited
64 cultivation periods without complete biofilm maturation [19–21]. Other approaches involve the separate
65 cultivation of skin tissue and bacteria until biofilm maturation. As translocation of an intact biofilm cultivated in

66 traditional model systems is impossible due to insufficient mechanical stability, biofilm fragments are transferred
67 to the skin tissue [22]. However, as the complex biofilm architecture including the protective matrix significantly
68 contributes to the overall properties of the biofilm and its resistance to antibiotics, such models unfortunately
69 lack predictability for the situation in the human body, especially for testing of novel antibiotics. To overcome
70 this issue, a biofilm model based on a three-dimensional fiber matrix was successfully developed, for the first
71 time enabling the non-destructive transfer of a mature biofilm to tissue models [23].

72 Altogether, the number of studies conducted on *in vitro* models of biofilm-infected wounds is scarce and
73 generally of limited predictability. In order to identify an appropriate model for future basic or translational
74 studies in this research field, it is crucial to investigate which aspects of the biofilm-host interactions can be
75 assessed with the different tissue models, the degree of comparability of the results and their translatability to
76 the human *in vivo* situation. For addressing this knowledge gap, we infected human *in vitro* and *ex vivo* wound
77 models with intact, matured *P. aeruginosa* biofilms and investigated them regarding morphology, host-pathogen
78 interactions and the response of the wound models to biofilm infection.

79 2 Materials and Methods

80

81 2.1 Materials

82 EpidermFT™ human *in vitro* skin models (antibiotic-free and antifungal-free media) were supplied by MatTek In
83 Vitro Life Sciences Laboratories, s.r.o. (Bratislava, Slovak Republic). Gelatin (from porcine skin, 300 Bloom, type
84 A), cellulose acetate (CA, Mn 30.000), and fetal calf serum (FCS) were purchased from Sigma-Aldrich (Steinheim,
85 Germany). Glacial acetic acid 100% and chloroform >99,8% were obtained from VWR International GmbH
86 (Darmstadt, Germany). Dulbecco's modified Eagle medium (DMEM), nutrient agar, Maxima H Minus First Strand
87 cDNA Synthesis Kit, and *Pseudomonas aeruginosa* (*P. aeruginosa*, ATCC 27853) were purchased from Thermo
88 Fisher Scientific GmbH (Dreieich, Germany). Dulbecco's phosphate-buffered saline (PBS) was supplied by Biowest
89 (Nuaillé, France). Formaldehyde methanol-free 30%, xylol > 97%, paraffin (Paraplast®), ethanol > 99,8%, eosin G
90 0.5%, and hematoxylin solution according to Mayer were purchased from Carl Roth GmbH & Co. KG (Karlsruhe,
91 Germany). Tri-Reagent was obtained by BIOZOL Diagnostica Vertrieb GmbH (Eching, Germany). Direct-zol™ RNA
92 MiniPrep Plus Kit including DNase I Set was supplied by Zymo Research Europe GmbH (Freiburg, Germany) and
93 PowerUp™ SYBR™ Green Master Mix was purchased from Applied Biosystems Deutschland GmbH (Darmstadt,
94 Germany).

95

96 2.2 Preparation of human *ex vivo* and *in vitro* wound models

97 For the *ex vivo* models, human skin tissue was obtained from Caucasian adults, undergoing reduction surgery
98 (Clinic for plastic and aesthetic surgery, reconstructive and hand surgery, Agaplesion Markus Krankenhaus,
99 Frankfurt, Germany). The present study was approved by the local ethics committee (ethics commission of the
100 state medical chamber, Hessen, 2020-1899-AF) and all skin donors gave their written informed consent. Skin
101 explants were further processed within approximately 2 h after excision. Briefly, after removal of the
102 subcutaneous fatty tissue, the skin tissue was either frozen at -21 °C for a minimum of 2 days, representing the
103 status "non-viable *ex vivo* models" or immediately further processed for tissue culture to maintain viability,
104 delineating the "viable *ex vivo* models" investigation group. To assure reproducible wounding conditions, the
105 skin was stretched using an in-house developed device (Fig. S1) and full-thickness wounds were created by taking
106 a standardized punch biopsy of 3 mm diameter. Subsequently, round-shaped 12 mm tissue punch samples
107 comprising the wound surrounded by intact skin were transferred to sterile gauze soaked with DMEM + 10% FCS
108 within a 12-well plate to allow for air-liquid cultivation and incubated overnight at 37 °C and 5% CO₂. All
109 experiments with *ex vivo* wound models (non-viable / viable) were conducted in triplicate with three different
110 donors.

111 Commercially available *in vitro* skin models (EpidermFT™) were wounded according to the manufacturer's
112 protocol [24]. Similar to the *ex vivo* models, wounds were created with a sterile 3 mm biopsy punch and wounded
113 samples were incubated overnight at 37 °C and 5% CO₂ in antibiotic-free and antifungal-free maintenance
114 medium, provided by the manufacturer.

115

116 2.3 Preparation of biofilms and biofilm-infected wounds

117 Mature biofilms of *P. aeruginosa* were prepared as previously described [23]. Briefly, electrospun fiber scaffolds,
118 equally composed of cellulose acetate and gelatin, were fabricated via blend electrospinning of a homogenous
119 solution of both polymers in 90% acetic acid. Process parameters for fabrication were selected according to the
120 aforementioned publication. The electrospun scaffolds were subsequently inoculated with *P. aeruginosa* and
121 cultivated on modified nutrient agar plates, containing 20% FCS, at 37 °C. After 48 h cultivation, mature biofilms
122 were used for further experiments. For wound infection, 3 mm punch biopsies of the mature biofilms were
123 transferred onto the wound bed of the *ex vivo* and *in vitro* wound models. The infected wound models were
124 incubated at 37 °C and 5% CO₂ until further analysis.

125

126 2.4 Histology

127 Histological analysis of infected *ex vivo* wound models (non-viable / viable) was performed after 3, 6, 10, 24,
128 and 48 h while the infected *in vitro* wound models were assessed after 3, 10, and 24 h. In parallel, samples of
129 uninfected, wounded models of each skin tissue condition were taken as controls and processed accordingly.
130 Each tissue sample was fixed with 4% phosphate-buffered formaldehyde solution for 6 h at room temperature.
131 Afterwards, dehydration with an ascending ethanol series, clearing with xylol, and embedding in paraffin were
132 performed, followed by the preparation of tissue cross sections measuring 5 µm in thickness using a rotary
133 microtome (Cut 6062, SLEE medical GmbH, Nieder-Olm, Germany). In the next step, tissue sections were stained
134 with hematoxylin according to Mayer and eosin G, following the manufacturer's protocol. Single micrographs
135 were acquired with the bright field mode of a confocal laser scanning microscope (LSM 900, Carl Zeiss Microscopy
136 GmbH, Jena, Germany) with the Axiocam 506 color camera (Carl Zeiss Microscopy GmbH, Jena, Germany) and a
137 10x objective (numeric aperture: 0.45, Plan-Apochromat, Carl Zeiss Microscopy GmbH, Jena, Germany).
138 Subsequently, micrographs were stitched using corresponding Zeiss Zen blue software. Three samples were
139 assessed for each condition to ensure accuracy and reliability of the results.

140

141 2.5 Raman spectroscopy

142 Label-free analysis of the biofilm infected *ex vivo* as well as *in vitro* skin tissues and uninfected controls was
143 performed by recording Raman spectra at 24 h of cultivation based on the identical paraffin-embedded wound
144 tissue samples as used for histological analysis. Tissue cross sections measuring 24 µm in thickness were mounted
145 onto CaF₂ glass slides followed by a deparaffinization step using a descending xylol / ethanol series. The dry
146 samples were analyzed using a WITec alpha 300R⁺ microscope (WITec GmbH, Ulm, Germany) coupled with a
147 532 nm diode laser, which was adjusted to a power of 3.0 mW in front of the objective (50x, numeric
148 aperture: 0.8, EC Epiplan-Neofluar, Carl Zeiss Microscopy GmbH, Jena, Germany). Raman spectra of the dermis
149 and the epidermis of infected and uninfected wounded models were recorded with an integration time of 0.5 s
150 and 10 accumulations and a spectral resolution of 4 cm⁻¹ in a range of 400-3700 cm⁻¹. Background subtraction of
151 the spectra was performed using WITec Project Plus software (WITec GmbH, Ulm, Germany), the subsequent
152 preprocessing (normalization and cosmic ray removal) as well as the multivariate data analysis were conducted
153 in MATLAB (Version R2023a, MathWorks, USA).

154

155 2.6 Quantification of colony forming units (CFUs)

156 To determine the colony forming units (CFUs) of *P. aeruginosa*, punch biopsies with a diameter of 6 mm were
157 taken from the infected *ex vivo* wound models after 3, 6, 10, 24, and 48 h of incubation, and from infected *in vitro*
158 wound models after 3, 10, and 24 h of incubation. The samples included the entire biofilm-infected wounds and
159 surrounding tissue. The skin samples were placed in centrifuge tubes filled with zirconia beads (1.4 - 1.6 mm) and
160 homogenized with a bead mill homogenizer (Bead Mill MAX, VWR International GmbH, Darmstadt, Germany).
161 Aggregates of bacteria were disrupted with sonication for 2 min to obtain a single cell suspension of
162 *P. aeruginosa*. Subsequently, serial 10-fold dilutions were prepared with sterile PBS and plated on nutrient agar
163 plates. Visible colonies were counted after 24 h incubation at 37 °C. The experiments were performed in
164 triplicate.

165

166 2.7 Scanning electron microscopy (SEM)

167 For visualization of the biofilm morphology and the host-pathogen interface as represented by the wound bed
168 after biofilm removal, samples of infected viable and non-viable *ex vivo* wound models were collected and fixed
169 as described above. After dehydration using an ascending ethanol series, tissues were divided in half and biofilms
170 were detached from one section to reveal the infected wound bed. Following complete ethanol removal by
171 critical point drying (Leica EM CPD300 Automated Critical Point Dryer, Leica Mikrosysteme GmbH, Vienna,
172 Austria), the samples were mounted on carbon tapes and sputter-coated with gold / palladium (80% / 20%) for
173 three minutes (SC7620, Quantum Design GmbH, Darmstadt, Germany). Micrographs were acquired at a
174 magnification of 2,000x and an acceleration voltage of 8 kV using a scanning electron microscope (EVO 10, Carl
175 Zeiss Microscopy GmbH, Jena, Germany) at room temperature.

176

177 2.8 Analysis of cytokine gene expression

178 For determining the gene expression of the selected cytokines and chemokines IL-1 β , IL-6, IL-8, and TNF α via
179 RT-qPCR, 3 mm biopsy punches of the infected wounds were obtained from viable *ex vivo* models after 3, 6, 10,
180 and 24 h and from *in vitro* models after 3, 10, and 24 h. As controls, samples of uninfected wound models were
181 taken at the mentioned time points, accordingly. Immediately after collection, the tissue pieces were snap-frozen
182 in liquid nitrogen and stored at -80 °C until further processing. Prior to RNA isolation, samples were placed in
183 Tri-Reagent and homogenized with zirconia beads (2.8 mm) using a bead mill homogenizer (Bead Mill MAX, VWR
184 International GmbH, Darmstadt, Germany). Furthermore, samples were washed with chloroform to optimize
185 RNA yield and purity [25]. Total RNA was isolated using the Direct-zol™ RNA MiniPrep Plus Kit, following the
186 manufacturer's instructions. To impede contamination with genomic DNA, digestion with DNase was also
187 performed. The final RNA concentration was determined using the NanoQuant plate in combination with a
188 microplate reader (Spark multimode microplate reader, Tecan, Männerdorf, Switzerland). RNA was stored at -
189 80 °C until cDNA synthesis, where 100 ng RNA was transcribed using the Maxima H Minus First Strand cDNA
190 Synthesis Kit. Notably, solely oligo (dT)₁₈ primers were applied in order to exclusively transcript eucaryotic mRNA

191 and avoid bacteria-derived cDNA production. cDNA was quantified as already described for total RNA and stored
 192 at -80 °C. RT-qPCR experiments were performed with the PowerUp™ SYBR™ Green Master Mix, according to the
 193 manufacturer's protocol, on a Real-Time PCR System (StepOnePlus, Applied Biosystems Deutschland GmbH,
 194 Darmstadt, Germany). The applied gene-specific primer sequences are listed in Table 1 (generated with primer-
 195 blast, National Center for Biotechnology Information, NCBI). Relative gene expression was assessed by
 196 normalizing to GAPDH, relating the Ct values to the corresponding uninfected control and determining fold
 197 changes according the $2^{-\Delta\Delta Ct}$ method described by Livak and Schmittgen [26]. For each infected wound condition
 198 and time point, three samples were assessed.

199 **Tab. 1: Primers for RT-qPCR**

Primer	Sequence (5'→ 3')
GAPDH	forward: CGGGAAGCTTGTCATCAATGG reverse: GGCAGTGATGGCATGGACTG
IL-1β	forward: AGCTACGAATCTCCGACCAC, reverse: CGTTATCCCATGTGTCGAAGAA
IL-6	forward: ACTCACCTCTCAGAACGAATTG reverse: CCATCTTTGGAAGGTTTCAGGTTG
IL-8	forward: GAGAGTGATTGAGAGTGGACCAC reverse: CACAACCCTCTGCACCCAGTTT
TNFα	forward: CCTCTCTAATCAGCCCTCTG reverse: GAGGACCTGGGAGTAGATGAG

200

201 2.9 Statistical analysis

202 CFU data is shown as mean \pm standard deviation, calculated with Microsoft Office Excel. For RT-qPCR data, error
 203 bars were calculated according to Livak and Schmittgen [26] and statistical analyses were carried out based on
 204 ΔCt values. Two-tailed unpaired student-T tests were performed using Microsoft Office Excel for all statistical
 205 evaluations. The results were considered statistically significant when $p < 0.05$ (* $p < 0.05$,
 206 ** $p < 0.01$, *** $p < 0.001$).

207 3 Results

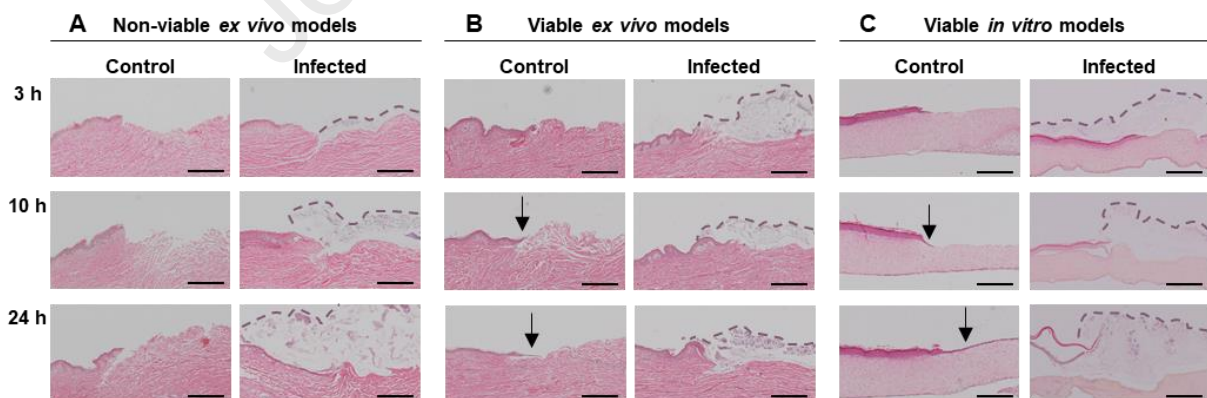
208 3.1 Histological characterization of biofilm-infected 3D wound models

209 After inoculation with mature *P. aeruginosa* biofilms, non-viable and viable *ex vivo* as well as viable *in vitro*
 210 models and their respective controls were subjected to histological characterization based on hematoxylin and
 211 eosin staining with particular focus on structural appearance and host-pathogen contact after biofilm infection.
 212 The images presented in Figure 1 are representative for three samples analyzed for each condition.

213 To assure adequate tissue integrity before biofilm infection, uninfected tissue samples of all three wound model
 214 types were analyzed regarding their three-dimensional morphological appearance and structural intactness. In
 215 all three wound models, well-defined epidermal and dermal layers were observed. Furthermore, no signs of cell
 216 deformation or tissue disruption due to the freeze-thawing process were detected in the non-viable *ex vivo* skin.
 217 A remarkable difference between the *in vitro* and *ex vivo* models was noticed in thickness and structure of the
 218 dermis. While the *ex vivo* dermis reached a thickness of up to 5000 μm , the *in vitro* dermis showed a maximum
 219 thickness of 750 μm and appeared more homogeneous and denser. The wound size slightly varied, both within
 220 and between the different models.

221 For the viable *ex vivo* and *in vitro* models, wound healing in form of re-epithelialization occurred (Fig. 1B and 1C).
 222 While the wounded area of the *in vitro* model was completely re-epithelialized after 24 h, wound healing in the
 223 *ex vivo* model was limited to an epithelial tongue reaching into the wound bed.

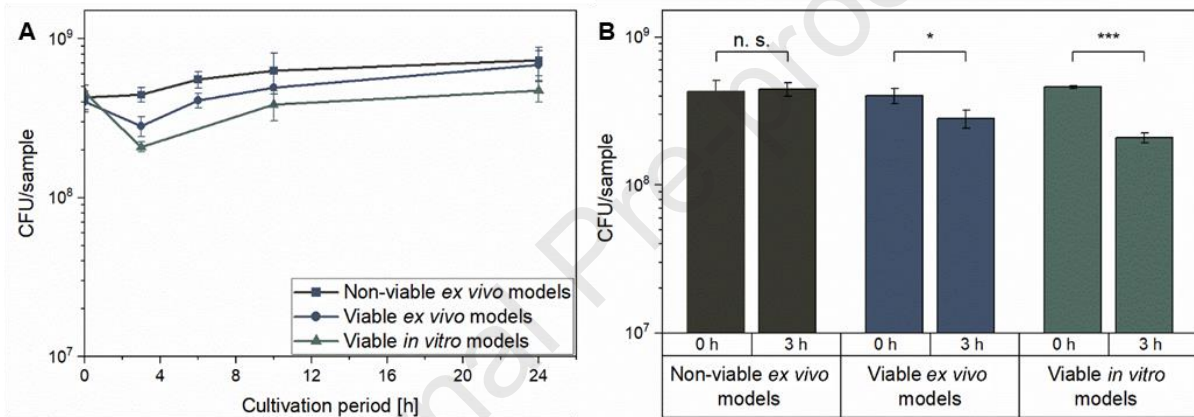
224 The images obtained from the infected models revealed close contact between the biofilm and the wound bed
 225 for all models with an increase in biofilm density over time. Disruption of the tissue structure became apparent
 226 after 10 h in all models. Specifically, the *stratum corneum* constituting the uppermost layer of the human skin
 227 was detached from the skin due to partial epidermolysis. This effect further intensified in the remaining
 228 observation period.



229
 230 **Fig. 1: Representative brightfield images of hematoxylin & eosin-stained paraffin sections of uninfected**
 231 **controls and infected wound models: (A) non-viable *ex vivo* models, (B) viable *ex vivo* models, and (C) *in vitro***
 232 **models.** Infected wound models were inoculated with mature *P. aeruginosa* biofilms and samples for histological
 233 analysis were collected after 3, 10, and 24 h incubation period. *P. aeruginosa* biofilms are bordered with dashed
 234 lines as guide to the eye and arrows indicate areas of re-epithelialization. Scale bar = 500 μm .

235 3.2 Quantification of biofilm growth behavior in dependency of host-pathogen interactions

236 To assess the impact of direct host-pathogen interactions of the different wound models on the bacterial growth
 237 behavior, quantification of CFUs was performed after inoculation with mature *P. aeruginosa* biofilms, comprising
 238 approximately $4.5 \cdot 10^8$ viable bacteria. Infected *ex vivo* as well as *in vitro* wound models were investigated after
 239 3, 6, 10, and 24 h or 3, 10, and 24 h, respectively (Fig. 2A). In the case of non-viable *ex vivo* models, the number
 240 of *P. aeruginosa* steadily increased up to $6.3 \cdot 10^8$ ($\pm 1.8 \cdot 10^8$) bacteria per wound after 10 h, followed by a
 241 stationary phase. The results for the viable *ex vivo* and *in vitro* models revealed a significant decrease in bacterial
 242 viability at 3 h (Fig. 2B), with CFUs dropping to $2.8 \cdot 10^8$ ($\pm 4.6 \cdot 10^7$) and $2.0 \cdot 10^8$ ($\pm 1.5 \cdot 10^7$), respectively.
 243 However, bacterial counts increased thereafter. Notably, for the viable *ex vivo* models, the number of CFUs
 244 exceeded the starting value already after 6 h with $4.9 \cdot 10^8$ ($\pm 1.1 \cdot 10^8$) bacteria per wound. By 24 h, the number
 245 of CFUs was comparable to that of the non-viable *ex vivo* models. In contrast, the bacterial count remained lower
 246 for the biofilm-infected *in vitro* models, reaching $4.7 \cdot 10^8$ ($\pm 7.3 \cdot 10^7$) CFUs after 24 h.

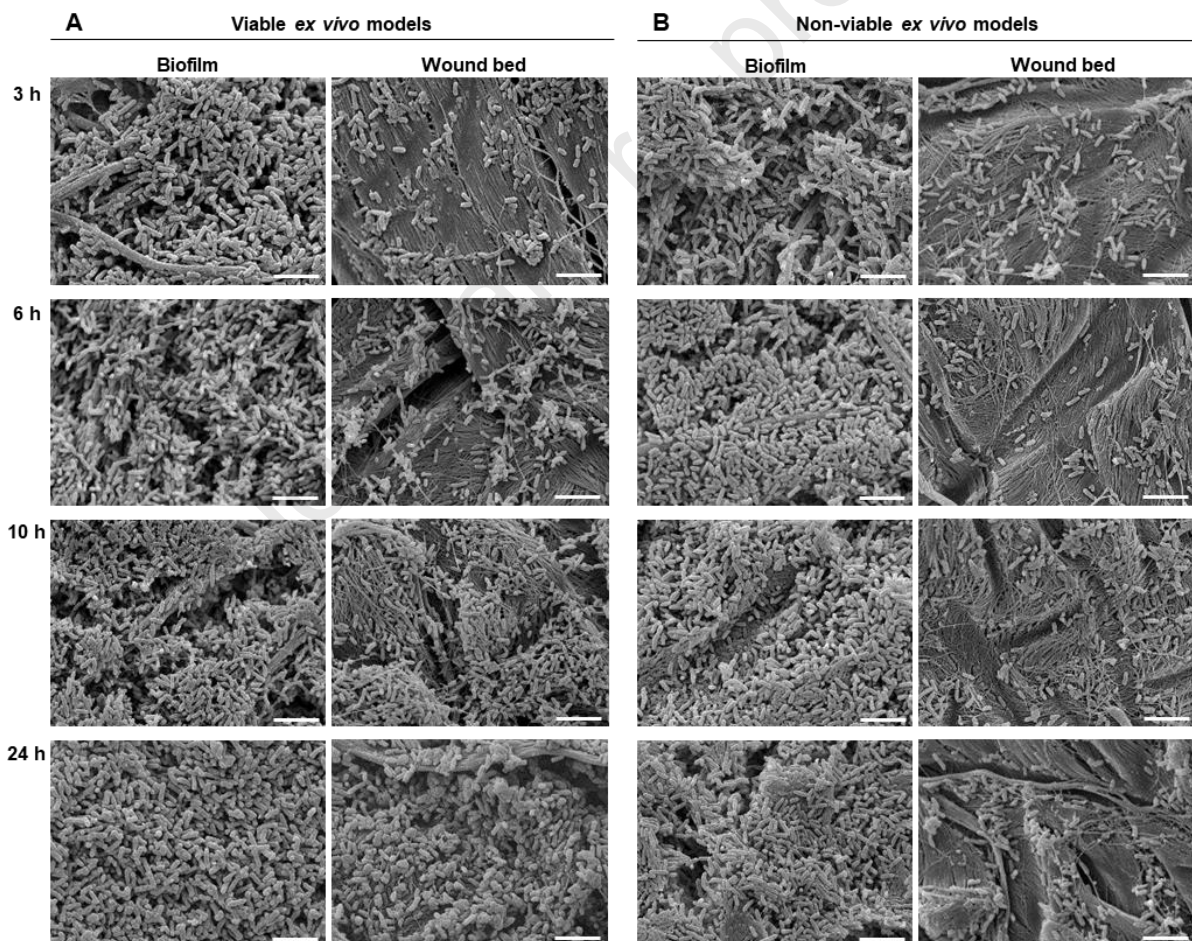


247

248 **Fig. 2: Evaluation of colony forming units (CFUs) to monitor bacterial growth of *P. aeruginosa* on viable *ex vivo***
 249 **models, non-viable *ex vivo* models, and viable *in vitro* models of human wounds.** (A) CFUs were determined at
 250 0, 3, (6), 10 and 24 h after infection with mature biofilms. (B) The changes in viable bacterial counts from 0 to 3 h
 251 were statistically evaluated using two-tailed unpaired student T tests with * $p < 0.05$, ** $p < 0.01$, *** $p < 0.001$.
 252 All results are shown as mean with standard deviations and all experiments were conducted in triplicate.

253 3.3 SEM analysis of biofilm morphology and bacterial growth patterns influenced by model viability

254 The growth and colonization patterns of *P. aeruginosa* biofilms on viable and non-viable *ex vivo* wound models
 255 were additionally examined by SEM in order to determine the effect of model viability on the interactions with
 256 biofilm bacteria. Micrographs of the biofilms and the wound beds after biofilm removal were obtained at
 257 different time points (after 3, 6, 10, and 24 h), as shown in Figure 3. After 3 h, a homogenous and dense bacterial
 258 growth was observed for all biofilms, independent of the underlying wound model. At this time point, nanofibers
 259 of the electrospun scaffolds were still visible. Over time, the biofilms appeared denser, with no discernible
 260 differences between the two wound models. After removal of the biofilms, imprints of electrospun fibers on the
 261 wound beds became visible in bacteria-free areas. Already after 3 h incubation, all wounds were colonized by
 262 individual bacteria, which began to form colonies from 6 h. By 10 h, bacterial growth patterns varied considerably
 263 between the two models. On viable excised skin, extensive colonization and the formation of larger aggregates
 264 were observed (Figure 3A). In contrast, significantly fewer bacteria were present on the wound beds of non-
 265 viable *ex vivo* models, mostly growing as individual cells (Figure 3B).



266

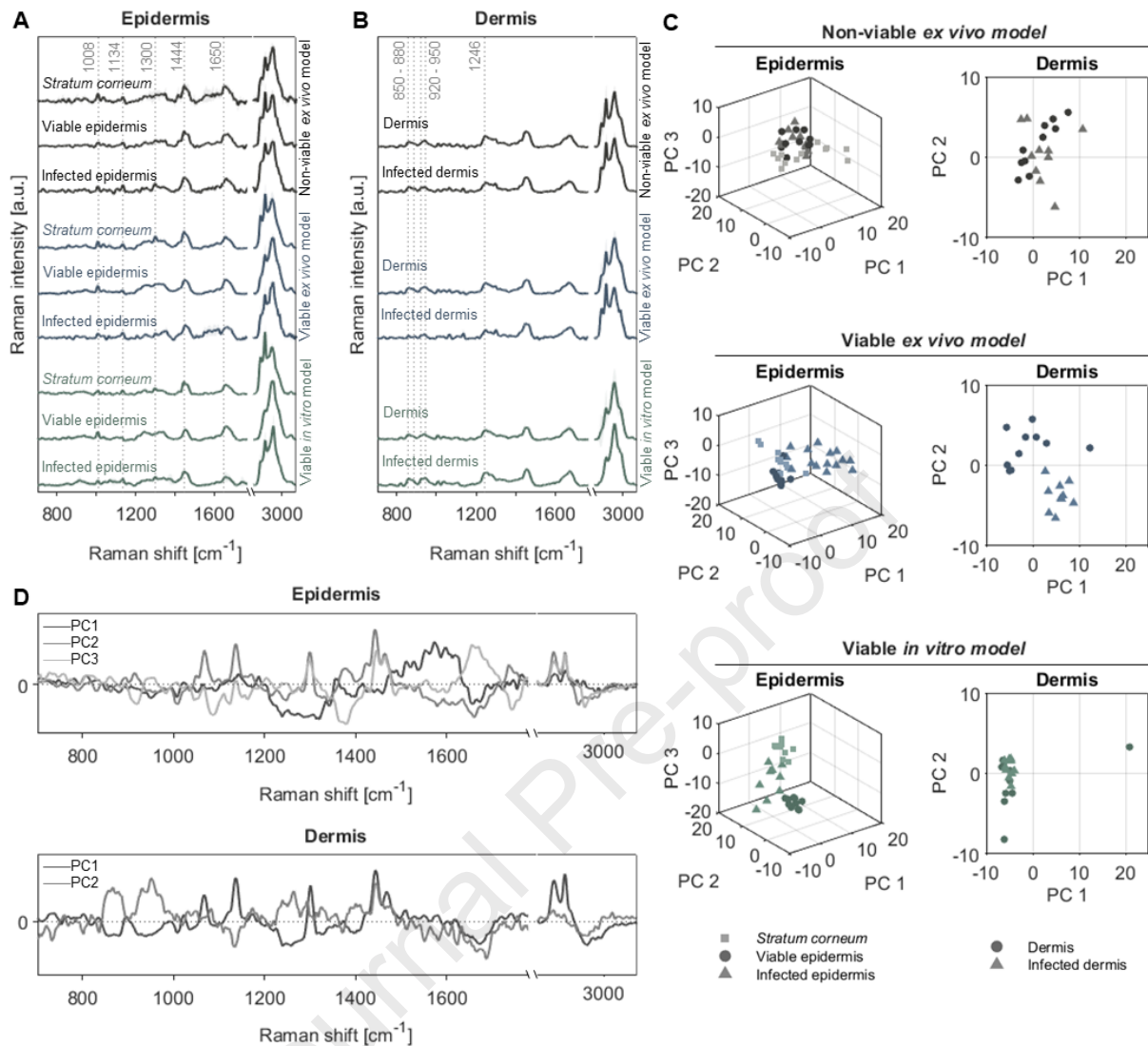
267 **Fig. 3: Assessment of biofilm morphology and bacterial growth pattern on wound beds after biofilm removal**
 268 **using scanning electron microscopy (SEM).** (A) Viable *ex vivo* wound models as well as (B) non-viable *ex vivo*
 269 wound models were infected with *P. aeruginosa* biofilms and cultivated for 3, 6, 10 and 24 h prior to SEM
 270 analysis. A magnification of 2,000x and an acceleration voltage of 8 kV were applied. Scale bar = 5 μ m.

271 **3.4 Investigation of the model composition and changes induced by biofilm infection using Raman spectroscopy**
272 Raman spectra were collected from cross sections of infected and uninfected models after 24 h of cultivation.
273 Differences in the tissue composition between the wound models, as well as in response to the biofilm infection
274 on a molecular level were assessed. For the analysis of the viable and the non-viable *ex vivo* model, samples of
275 the same donor were selected, respectively. Spectra were acquired in the wounded area from the remaining
276 epidermis and dermis of the infected models and compared to spectra obtained from the *stratum corneum*, the
277 viable epidermis and dermis of the uninfected control models.

278 The Raman spectra of the epidermal regions primarily exhibited Raman signals associated with proteins and lipids
279 (Fig. 4A). In detail, Raman signals at 1008 cm^{-1} , 1444 cm^{-1} , and 1650 cm^{-1} represented the vibrational modes of
280 aromatic amino acids, the deformation of C-H bonds and the carbonyl group (C=O) vibration of amide I,
281 respectively [27,28]. Additional signals observed at 1134 and 1300 cm^{-1} were attributed to the vibration of C-C
282 bonds of lipids with skeletal trans conformation and the deformation of C-H2 bonds of lipids [27]. C-H stretching
283 modes, corresponding to lipid alkyl chains, were assigned to signals in the range of 2850-2950 cm^{-1} [29]. The
284 Raman spectra of the dermal regions are additionally characterized by two double peaks at 850 to 880 cm^{-1} and
285 920 to 950 cm^{-1} , corresponding to C-C stretching of the protein backbone and the proline / hydroxyproline ring
286 of collagen, and a distinct signal at 1246 cm^{-1} , representing the C-N stretching of amide bonds (Fig. 4B) [30].

287 The differences between the *ex vivo* and the *in vitro* models, as well as between the respective infected and
288 uninfected models, were assessed using principal component analysis (PCA). The PCA was independently
289 conducted with the epidermal spectra and the dermal spectra. Subsequent Pareto plots revealed that three
290 principal components (PCs) explained more than 50% of the total variability of the epidermal spectra (PC 1:
291 26.3%, PC 2: 14.4%, PC 3: 10.3%), while two principal components explained more than 50% of the total
292 variability of the dermal spectra (PC 1: 39.0%, PC 2: 12.1%) (Fig. S2). For clarity, the scores of the different models
293 were plotted separately (Fig. 4C). The score plots of the epidermal spectra indicated that the *stratum corneum*,
294 the viable and the infected epidermis can be distinguished on the basis of their Raman signals in case of the
295 viable *ex vivo* model and the *in vitro* model. However, no clear separation of the groups was apparent for the
296 non-viable *ex vivo* model. Further, compared to the *in vitro* model, both *ex vivo* models exhibited greater
297 variability in the Raman spectra. The latter observation also applied to the score plots of the dermal spectra.
298 Despite of the signal heterogeneity, distinct clusters of Raman spectra of the infected and uninfected samples
299 were observed for the viable *ex vivo* model. In contrast, neither the score plot of the non-viable *ex vivo* model
300 nor that of the *in vitro* model exhibited a clear separation of the dermal spectra.

301 The PC loading plots revealed discriminant wavenumbers, reflecting different components of the tissue analyzed
302 (Fig. 4D). Epidermal samples with a positive PC 1 score were correlated with an increase of the amide II signal,
303 conversely, a negative PC 1 score indicated an elevated amide III signal. PC 2 was assigned to the relation of lipids
304 (positive scores) to proteins (negative score), while PC 3 depicted the ratio between overall protein (positive
305 score) and DNA Raman signals (negative score). Regarding the PCA of the dermal spectra, a positive PC 1 score
306 was associated with lipids, whereas proteins were reflected by a negative PC 1 score. Differences in the collagen
307 composition of the tissues were visualized by PC 2 (positive score). A full peak assignment can be found in the
308 supporting information (Tab. S1).

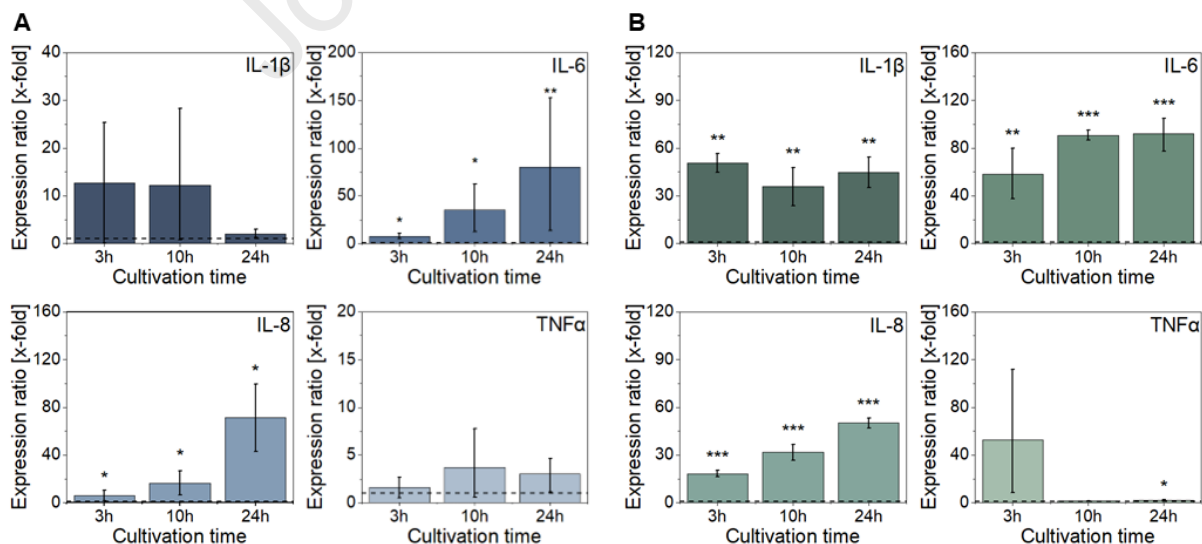


309

310 **Fig. 4: Investigation of the tissue composition of the human-derived wound models and their response to**
 311 **biofilm infection after 24 h using Raman spectroscopy. (A) Mean spectra of the *stratum corneum*, the viable**
 312 **epidermis and the infected epidermis and (B) the dermis and the infected dermis of the viable and the non-viable**
 313 ***ex vivo* model as well as the viable *in vitro* model. (C) Score plots of the principal component analysis of the**
 314 **epidermal and the dermal spectra and (D) corresponding loading plots.**

3.5 Evaluation of cytokine gene expression representing pro-inflammatory mediators of the immune response

To analyze the innate immune response of the different wound models to the biofilm infection, the time-dependent gene expression of selected pro-inflammatory cytokines and chemokines, namely IL-1 β , IL-6, IL-8, and TNF α , was evaluated in viable *ex vivo* and *in vitro* skin wound models infected with *P. aeruginosa* biofilms after 3, 6, 10, and 24 h or 3, 10 and 24 h, respectively. The RT-qPCR results of biofilm-infected *ex vivo* wound models are shown in Figure 5A. In the case of IL-1 β , already after 3 h high expression levels of 12.7 (\pm 12.6) could be observed, even though this increase in fold changes was not statistically significant. Notably, the lowest expression levels were found after 24 h incubation. For IL-6 and IL-8, RT-qPCR results revealed significantly higher gene expression levels during biofilm infection compared to the uninfected control for all time points examined. While the upregulation of IL-6 was already pronounced after 10 h reaching fold changes of 35.2 (+26.9 / -23.1) and remained relatively stable thereafter, gene expression of IL-8 peaked at 24 h with fold changes of 71.2 (\pm 28.2) after showing low levels at the previous time points. Throughout the study, only low gene expressions of TNF α were observed compared to the control with fold changes reaching from approximately 1.5 to 3.7. In general, high standard deviations were revealed for the experiments conducted with *ex vivo* wound models. For experiments with the *in vitro* wound models, RT-qPCR results are shown in Figure 5B. Gene expressions of biofilm-infected *in vitro* skin wounds showed similarities in cytokine expression after 3, 10 and 24 h of biofilm infection compared to the *ex vivo* skin. IL-1 β , IL-6, and IL-8 were significantly upregulated at all time points upon infection. While for IL-1 β and IL-6 high and stable fold changes were obtained over the total investigated period with maximal values of 50.5 (\pm 5.9) and 92.0 (\pm 14.8), respectively, IL-8 expression rose over time and reached a maximal fold change of 50.3 (\pm 3.3) after 24 h. Again, minimal upregulation of TNF α was observed for the later time points, while high fold changes of 52.8 (\pm 44.4) occurred after 3 h. With a few exceptions, standard deviations were low for the experiments with the commercially available *in vitro* skin models.



338

339 **Fig. 5: Gene expression of pro-inflammatory cytokines in response to biofilm infection by RT-qPCR.** (A) Viable
 340 *ex vivo* wound models as well as (B) *in vitro* wound models were infected with mature *P. aeruginosa* biofilms and
 341 gene expressions of IL-1 β , IL-6, IL-8, and TNF α were determined after 3, 10, and 24 h cultivation. The dashed line
 342 indicates a fold change of 1. The mean expression ratio and error bars were calculated according to the $2^{-\Delta\Delta C_t}$

343 method [31]. For statistical analysis, two-tailed unpaired student T tests based on ΔC_t values was performed,
344 comparing the infected samples with the corresponding uninfected control (* $p < 0.05$, ** $p < 0.01$, *** $p < 0.001$).

Journal Pre-proof

4 Discussion

In the past, *in vitro* biofilm models cultivated in artificial environments were crucial for obtaining valuable fundamental molecular and mechanistic insights into the formation and maturation of bacterial biofilms, but unfortunately, certain limitations persist as they fail to reflect the interaction of biofilm and biological tissue present in the complex *in vivo* scenario [32]. Understanding this interplay is essential for the rational development and testing of effective therapeutics against wound infections. Consequently, it is imperative to create a suitable model that represents both components, the biofilm and the affected tissue. While it is ethically impossible to include humans in preclinical biofilm-related wound infection studies, the utilization of animal test models also poses several significant drawbacks including limited predictability to the human *in vivo* situation, due to substantial interspecies differences in structural composition as well as in immune and wound healing mechanisms [7,8]. Against this background, an urgent need for predictive alternative human-based infection models becomes evident. Yet, the accurate imitation of the biofilm-infection state of wound infections *in vitro* remains challenging, due to detrimental effects of relevant bacteria on the host tissue during biofilm maturation [18]. Consequently, current human-derived *in vitro* infection models mainly focus on the sole replication of the initial infection phase caused by planktonic bacteria, while assessment of more advanced infection stages with biofilm formation and corresponding host-pathogen interactions still depend on animal models. To cover this gap, a mature biofilm model based on an electrospun scaffold was developed, which can be transferred to *in vitro* tissue models without destruction [23]. In this study, a comparative approach of biofilm-infected wound models was employed by combining mature biofilms with different human *ex vivo* and *in vitro* wound models of varying complexity. A pre-cultivation period of 48 h was selected to attain biofilm maturity, which was previously verified by the emergence of crucial structural and functional biofilm characteristics [23]. Simultaneously, the cultivation separately from the wound tissue was kept as short as possible to minimize the potential influence of abiotic elements of the *in vitro* setting on biofilm development. For the first time, intact and mature *P. aeruginosa* biofilms were used to induce advanced infections on wounded human *ex vivo* skin models (viable and non-viable) as well as on commercially available human *in vitro* skin models (EpidermFT™, MatTek In Vitro Life Sciences Laboratories, s.r.o). The infected wound models were subsequently investigated regarding morphology, host-pathogen interactions and the response of the wounded skin tissue to biofilm infection. This comprehensive analysis aimed at assessing the translatability of these models to the human body, while simultaneously identifying appropriate application fields for the different models under investigation.

Based on histochemical analysis of the infected and uninfected models, detailed information in terms of morphological tissue characteristics and structural changes induced by biofilm infection could be attained. Each wound model comprised the complex three-dimensional and hierarchically structured morphology of human skin characterized by a multi-layered epidermis with a cornified top-sheet and an underlying dermal compartment. Adverse effects on tissue integrity of the non-viable *ex vivo* models following freezing at -20 °C and subsequent thawing could not be observed, which is in good accordance with the literature [19]. This represents a non-negligible aspect, as tissue integrity loss during model preparation impedes the identification of destructive effects caused by bacterial biofilms. Accordingly, these findings corroborated the general applicability of freeze-thawed wound models for evaluation of structural changes during infection. Differences

383 in thickness and structural complexity of the dermal compartment between the *ex vivo* and *in vitro* models could
384 affect the spatial-temporal penetration behavior of bacteria and nutrients. However, visible differences in terms
385 of bacterial invasion were not apparent. In addition, no adverse impact on epidermal-dermal cross-
386 communication as mandatory key event for re-epithelialization could be detected, as visualized by pronounced
387 epithelial tongue formation sprouting from the wound edges into the wound bed. As previously reported, the
388 altered dermal structure in *in vitro* models does not hinder cellular key interactions required for proper wound
389 healing [33]. Re-epithelialization as indicator for skin viability was observed in both, viable *ex vivo* and *in vitro*
390 control models, confirming a wound healing mechanism comparable to the human *in vivo* situation, in contrast
391 to murine models, where excisional wounds predominantly close by tissue contraction [8]. Confirming previous
392 findings, the analysis of the infected models revealed adequate biofilm attachment to the wound bed, thereby
393 promoting optimal conditions for host-pathogen interactions at the biofilm-tissue interface [23]. Hence, each
394 tested wound model was suitable to mimic the close contact between biofilm and tissue, thus being capable of
395 recapitulating the *in vivo* situation. The histological analysis further unveiled epidermolysis in all three infected
396 models, characterized by the loss of keratinocytes and detachment of the epidermis from the underlying tissue,
397 which is in line with literature knowledge [9,34]. Notably, this effect occurred in both, viable and non-viable
398 models, suggesting that the defense mechanisms of viable skin cells were not sufficient to effectively combat
399 biofilm-induced tissue disruption. From a histological perspective, all tested biofilm-infected wound models
400 served as suitable alternatives to animal testing if studying structural aspects is of interest. In this context,
401 commercial *in vitro* models can be advantageous due to greater availability in case of limited access to excised
402 tissue. Further, non-viable *ex vivo* models are an appropriate choice if the expertise to maintain skin viability
403 during culture is lacking.

404 Quantitative monitoring of the *P. aeruginosa* biofilm growth on the different wound models was assessed by
405 CFUs analysis. Results from infected, non-viable *ex vivo* wound models were in accordance with typical,
406 unhindered bacterial growth behavior in a nutrient-rich environment, characterized by an initial exponential
407 growth interval followed by a stationary phase. These findings aligned with existing literature that supports the
408 notion of *P. aeruginosa* providing various strategies for utilizing skin compounds as a source of nutrient supply
409 to promote bacterial growth [35,36]. Additionally, the lack of active defense mechanisms against bacterial
410 growth within the non-viable models allows for unhindered bacterial growth. Interestingly, bacterial growth was
411 initially impeded on infected viable wound models resulting in reduced numbers of viable *P. aeruginosa* at 3 h.
412 This effect was particularly pronounced for the *in vitro* wound models. Since these models lack immune cells, the
413 observed defense mechanism was predominantly originating from resident skin cells, such as keratinocytes and
414 fibroblasts. In this context, one important component of the first-line defense cascade in response to bacterial
415 infection is the production of antimicrobial peptides (AMPs), particularly by epithelial cells [37]. AMPs produced
416 by human keratinocytes have been shown to exhibit antibacterial activity against *P. aeruginosa* in both,
417 planktonic and biofilm phenotypes, and thus may contribute to the observed significant loss of bacterial viability
418 in early infection [38,39]. Detection of such effects using animal models is restricted due to interspecies
419 differences in the quantity and variety of AMPs [40]. In the *ex vivo* models, an additional effect of active immune
420 reactions by immune cells was conceivable. However, complete eradication of bacterial biofilms was not

421 observed due to e.g., the lack of a vascular system, restricting adaptive immune mechanisms [41]. In all *in vitro*
422 and *ex vivo* models, biofilms were able to recover and to persist, resulting in biofilm-related, advanced states of
423 wound infections. The slightly reduced number of viable *P. aeruginosa* bacteria observed on *in vitro* models after
424 24 h could be attributed to a reduced supply with nutrients due to their denser dermis structure impeding
425 diffusion. Furthermore, the composition of the collagen matrix might affect its degradation and metabolism
426 by bacteria.

427 The CFU analysis demonstrated that inoculation with mature *P. aeruginosa* biofilms resulted in a manifest wound
428 infection on all tested models, since, at all time points, the total bacterial load exceeded the critical level of
429 10^5 bacteria/g tissue, indicating manifest tissue infections [42]. For a detailed view, SEM micrographs of the
430 biofilms and of the underlying wound beds were acquired for viable and non-viable *ex vivo* models. Consistent
431 with previous reports, the biofilms were characterized by a homogenous bacterial distribution including dense
432 aggregates on the nanofiber scaffolds [23]. Biofilm density steadily rose during the incubation time, without
433 reflecting the initial reduction in bacterial viability on viable wound models observed by CFU analysis. This can
434 be attributed to captured dead bacteria in the biofilm matrix being not distinguishable from viable ones by SEM
435 visualization. While no significant differences in bacterial growth patterns within the biofilms were detected
436 among the two wound models, variations in bacterial growth behavior on the wound beds were apparent,
437 depending on the viability status of the models. After 24 h, the formation of microcolonies in the wound beds of
438 viable *ex vivo* models was consistent with the reported growth patterns of biofilms in clinical samples of human
439 chronic wound infections [43,44]. Consequently, the predominant presence of individual bacteria in the wound
440 beds of non-viable *ex vivo* models did not properly represent the *in vivo* situation. Previous literature suggests
441 that multiple factors may contribute to this phenomenon. Kirketerp-Møller et al. assumed that single bacteria
442 cannot withstand the hosts' immune responses, thus, the presence of active immune mechanisms forces the
443 bacteria to form microcolonies protecting them against external attacks [44]. The presence of pro-inflammatory
444 cytokines may also be relevant serving as stimulus for growth and biofilm formation of *P. aeruginosa* [45,46].
445 Even though general biofilm growth appeared similar on all wound models, our findings highlight the importance
446 of considering the wound viability status when investigating the pathogenesis of biofilm infections regarding
447 biofilm-host interactions.

448 Furthermore, confocal Raman microscopy was applied to gain deeper insights into biofilm-host interactions at a
449 molecular level, influenced by differences in wound model composition. With its non-invasive and chemically
450 selective working principle, Raman microscopy allowed for a detailed analysis of tissue components without the
451 need of labelling. Raman spectra of epidermal and dermal regions revealed chemically selective fingerprint peak
452 patterns, containing information about the tissue composition, the structure of single molecules as well as the
453 dynamics and interactions between different molecules. The peaks observed for the epidermal (represented by
454 keratin) and the dermal (represented by collagen) compartment of the uninfected control models were overall
455 consistent with previous studies [47,48]. However, the comparison of the models revealed varying peak ratios,
456 suggesting distinct differences in the composition of the tissue models. The spectra of the two viable models
457 showed similarities and reflected the terminal differentiation of keratinocytes in the viable part of the epidermis
458 to corneocytes in the upper *stratum corneum* based on a decrease in DNA-derived and a simultaneous increase

459 in protein-related Raman signals. No comparable findings were observed for non-viable *ex vivo* models. This can
460 be attributed to the fact that the keratinocytes already died during the freezing process of the wound model for
461 storage at -20°C. In the case of the dermal spectra, the *in vitro* model differed from both *ex vivo* models due to
462 a decreased variability in the spectra regarding the lipid / protein ratio, corresponding to the homogenous
463 appearance of the samples in the histological analysis. In a previous study, Ali et al. also applied Raman
464 microscopy on tissue sections of human skin and the EpidermFT™ *in vitro* model, reporting comparable spectra
465 of the epidermal and dermal layers [49]. To evaluate the response to the biofilm infection, the spectra of the
466 infected skin layers were compared to the corresponding uninfected control. Close similarities between the
467 spectra obtained from the infected and uninfected epidermal layers of non-viable *ex vivo* model can again be
468 explained by the prior cell death during freezing. In contrast, the viable *ex vivo* model exhibited the bacterial
469 damage of the epidermis by a decreased DNA Raman signal, which was comparable to the spectrum of the
470 *stratum corneum*. Additionally, the variability in the lipid / protein ratio increased, which also applied to the
471 infected epidermis of the *in vitro* model. However, while the spectrum of the viable *ex vivo* model is shifted
472 towards a higher lipid signal, the spectrum of the *in vitro* model moved towards an increased protein signal. This
473 difference was attributed to the fact that the epidermis of the *in vitro* model consisted exclusively of
474 keratinocytes, whereas the epidermis of the excised human skin is more complex and additionally contained
475 other cell types [49]. While for the dermal regions, no clear separation of the spectra groups was observed for
476 the non-viable *ex vivo* model, dermal spectra of the viable *ex vivo* model showed a decrease of the collagen
477 signal, indicating that collagen served as a nutrient source for bacteria. These pronounced changes were absent
478 in the dermis of the *in vitro* model, supporting together with the differences in the lipid / protein ratio the
479 hypothesis that compositional differences lead to a potentially reduced nutritional role compared to the *ex vivo*
480 model. Thus, for investigating compositional changes of the wounded tissue upon biofilm infections at a
481 molecular level, viable wound models proved to be particularly appropriate compared to the non-viable
482 counterparts. Moreover, while *ex vivo* models exhibited a more complex composition and a closer similarity to
483 the *in vivo* conditions, the advantage of commercial *in vitro* models lied in the lower variability.

484 In a next step, viable wound models (*ex vivo* / *in vitro*) were assessed regarding their capability to evoke an
485 *in vivo*-like human innate immune response induced by *P. aeruginosa* biofilm infection. Analysis of non-viable
486 *ex vivo* models was not conducted due to the absence of active defense mechanisms. Gene expression profile of
487 certain pro-inflammatory cytokines (IL-1 β , IL-6, TNF α) and a chemokine (IL-8) were evaluated as these
488 pro-inflammatory mediators play a significant role in the immune response during acute and chronic wound
489 infections [50–52]. Chronic wound infections, mostly biofilm-related, are generally associated with a prolonged
490 inflammatory phase exhibiting persistent high levels of pro-inflammatory cytokines [52]. The initial upregulation
491 of IL-1 β , a crucial early-phase cytokine, is in line with literature and could be demonstrated for both viable model
492 settings [53]. In contrast, the reduction of IL-1 β gene expression after 24 h in the *ex vivo* models deviated from
493 initial expectations for advanced, biofilm-related wound infections. However, it has been previously described
494 that *P. aeruginosa* provides different immunomodulating mechanisms, impeding the production of
495 pro-inflammatory cytokines including IL-1 β [54,55]. The reasons why this effect is solely observed in *ex vivo*
496 models remain not fully understood, probably due to the absence of immune cells, especially macrophages, in *in*

497 *vitro* models [56]. For both wound models, the observed high fold changes of IL-6 after 10 h (early phase of
498 infection), up to 24 h (persistent infection) were consistent with previous *in vivo* reports [53,57,58]. The detected
499 time-delayed increase in IL-8 expression can be attributed to its dependency on the prior expression of other
500 cytokines, in particular IL-1 β and TNF α [59]. The pro-inflammatory cytokine TNF α is reported to be extensively
501 secreted during the early phase of skin inflammation, followed by a rapid down-regulation thereafter [53]. In this
502 study, an early up-regulation could only be observed in case of *in vitro* models. For all subsequent time points,
503 the gene expression remained consistently low, thus mirroring *in vivo* observations. Overall, both, *ex vivo* and
504 *in vitro* models exhibited similar patterns of cytokine gene expression dynamics, aligning with literature reports
505 on human *in vivo* skin inflammation upon bacterial infection. The *ex vivo* models incorporating various cell types
506 capable of cytokine production including resident immune cells and non-immune skin cells (e.g., keratinocytes
507 and fibroblasts). A limited number of studies on immune response within infected *ex vivo* wound models exists,
508 reporting elevated levels of pro-inflammatory cytokines upon infection, as also observed in the present study
509 [9,60]. In contrast, commercially available *in vitro* models are characterized by their lack of harboring any
510 immune cells. Nevertheless, these *in vitro* models demonstrated high levels of pro-inflammatory cytokines,
511 highlighting the significant role of non-immune skin cells contributing to the innate skin immunity [50,61].
512 Previous *in vitro* studies using biofilm-conditioned media, demonstrated increased gene expression of
513 pro-inflammatory cytokines [62,63]. Further, data derived from *ex vivo* models revealed high standard deviations
514 due to a pronounced inter-individual variability, thus restricting reproducibility. Experiments conducted with
515 commercially available *in vitro* models showed a high level of reproducibility due to their well-defined
516 standardization in terms of model composition. Thus, the applicability of both viable wound models could be
517 proven for studying host immune responses to mature biofilm infections even though differing in immune
518 complexity.

519 In the present study, we identified the distinct strengths and advantages of biofilm-infected human
520 three-dimensional *ex vivo* and *in vitro* wound models differing in biological complexity, accompanied by exploring
521 the limitations of each model dependent on the scientific question of interest. The applicability of each presented
522 wound model for common investigation purposes encompassing the determination of bacterial growth and the
523 structural appearance could be verified to be independent of tissue viability status. However, we strongly
524 recommend the use of viable models, especially, when direct biofilm-skin tissue interactions are of major
525 interest. Due to a notable biological complexity of biofilm-infected *ex vivo* wound models, results derived from
526 these test settings possess a high predictive power for translation into a clinical setting. Hence, they are
527 particularly suitable in the context of fundamental research questions with focus on the multicellular interplay
528 in a complex, three-dimensional environment, thus paving the way for identification of new drug targets and
529 site-specific delivery strategies for anti-infective therapy. Commercially available *in vitro* models provide
530 precisely controlled tissue conditions including a well-defined compositional architecture, thus being superior
531 when a high degree of standardization and reproducibility are crucial factors, such as comparative drug screening
532 studies. In conclusion, our findings corroborate the great potential of the three-dimensional biofilm-infected
533 human wound models to be used across various application fields spanning from fundamental to translational
534 research purposes.

535 **Data availability statement:** The data underlying the findings of this study can be obtained from the
536 corresponding author with reasonable request.

537

538 **Conflict of interest:** The authors have no conflicts of interest to declare.

539

540 **Acknowledgements:**

541 We thank I. A. Ederer and U. Rieger from Agaplesion Markus Krankenhaus, Frankfurt, Germany for providing
542 excised human skin. Additionally, we would like to thank Nathalie Jung for her support.

543

544 **Funding:**

545 Funding was provided by Stiftung zur Förderung der Erforschung von Ersatz- und Ergänzungsmethoden zur
546 Einschränkung von Tierversuchen (set) (Grant number: P-070) and Deutsche Forschungsgemeinschaft (DFG,
547 German Research Foundation) (project number 414985841). This study was supported by the Cluster project
548 ENABLE funded by the Hessian Ministry for Science and the Arts.

549

550

551 **References**

- 552 [1] C.K. Sen, Human Wounds and Its Burden: An Updated Compendium of Estimates, *Adv. Wound Care (New*
553 *Rochelle)* 8 (2019) 39–48. <https://doi.org/10.1089/wound.2019.0946>.
- 554 [2] M. Malone, T. Bjarnsholt, A.J. McBain, G.A. James, P. Stoodley, D. Leaper, M. Tachi, G. Schultz, T. Swanson,
555 R.D. Wolcott, The prevalence of biofilms in chronic wounds: a systematic review and meta-analysis of
556 published data, *J. Wound Care* 26 (2017) 20–25. <https://doi.org/10.12968/jowc.2017.26.1.20>.
- 557 [3] R.D. Wolcott, D.D. Rhoads, S.E. Dowd, Biofilms and chronic wound inflammation, *J. Wound Care* 17 (2008)
558 333–341. <https://doi.org/10.12968/jowc.2008.17.8.30796>.
- 559 [4] K.N. Kragh, M. Alhede, L. Kvich, T. Bjarnsholt, Into the well-A close look at the complex structures of a
560 microtiter biofilm and the crystal violet assay, *Biofilm* 1 (2019) 100006.
561 <https://doi.org/10.1016/j.bioflm.2019.100006>.
- 562 [5] A.K. Seth, M.R. Geringer, S.J. Hong, K.P. Leung, T.A. Mustoe, R.D. Galiano, In vivo modeling of biofilm-
563 infected wounds: a review, *J. Surg. Res.* 178 (2012) 330–338. <https://doi.org/10.1016/j.jss.2012.06.048>.
- 564 [6] Bundesinstitut für Risikobewertung, Verwendung von Versuchstieren im Jahr 2021, 2022.
- 565 [7] J. Mestas, C.C.W. Hughes, Of mice and not men: differences between mouse and human immunology, *J.*
566 *Immunol.* 172 (2004) 2731–2738. <https://doi.org/10.4049/jimmunol.172.5.2731>.
- 567 [8] H.D. Zomer, A.G. Trentin, Skin wound healing in humans and mice: Challenges in translational research, *J.*
568 *Dermatol. Sci.* 90 (2018) 3–12. <https://doi.org/10.1016/j.jdermsci.2017.12.009>.
- 569 [9] L. Steinstraesser, M. Sorkin, A.D. Niederbichler, M. Becerikli, J. Stupka, A. Daigeler, M.R. Kesting, I. Stricker,
570 F. Jacobsen, M. Schulte, A novel human skin chamber model to study wound infection ex vivo, *Arch.*
571 *Dermatol. Res.* 302 (2010) 357–365. <https://doi.org/10.1007/s00403-009-1009-8>.
- 572 [10] T. Coenye, B. Kjellerup, P. Stoodley, T. Bjarnsholt, The future of biofilm research - Report on the '2019
573 Biofilm Bash', *Biofilm* 2 (2020) 100012. <https://doi.org/10.1016/j.bioflm.2019.100012>.
- 574 [11] V. Planz, C.-M. Lehr, M. Windbergs, In vitro models for evaluating safety and efficacy of novel
575 technologies for skin drug delivery, *J. Control. Release* 242 (2016) 89–104.
576 <https://doi.org/10.1016/j.jconrel.2016.09.002>.
- 577 [12] P. Kaiser, J. Wächter, M. Windbergs, Therapy of infected wounds: overcoming clinical challenges by
578 advanced drug delivery systems, *Drug Deliv. Transl. Res.* 11 (2021) 1545–1567.
579 <https://doi.org/10.1007/s13346-021-00932-7>.
- 580 [13] G. Brackman, T. Coenye, In Vitro and In Vivo Biofilm Wound Models and Their Application, *Adv. Exp.*
581 *Med. Biol.* 897 (2016) 15–32. https://doi.org/10.1007/5584_2015_5002.
- 582 [14] D.J. Yoon, D.R. Fregoso, D. Nguyen, V. Chen, N. Strbo, J.J. Fuentes, M. Tomic-Canic, R. Crawford, I.
583 Pastar, R.R. Isseroff, A tractable, simplified ex vivo human skin model of wound infection, *Wound Repair*
584 *Regen.* 27 (2019) 421–425. <https://doi.org/10.1111/wrr.12712>.
- 585 [15] A. de Breij, E.M. Haisma, M. Rietveld, A. El Ghalbzouri, P.J. van den Broek, L. Dijkshoorn, P.H.
586 Nibbering, Three-Dimensional Human Skin Equivalent as a Tool To Study *Acinetobacter baumannii*
587 Colonization, *Antimicrob. Agents Chemother.* 56 (2012) 2459–2464. <https://doi.org/10.1128/AAC.05975-11>.
- 588 [16] Rancan, Contardi, Jurisch, Blume-Peytavi, Vogt, Bayer, Schaudinn, Evaluation of Drug Delivery and
589 Efficacy of Ciprofloxacin-Loaded Povidone Foils and Nanofiber Mats in a Wound-Infection Model Based on
590 Ex Vivo Human Skin, *Pharmaceutics* 11 (2019) 527. <https://doi.org/10.3390/pharmaceutics11100527>.
- 591 [17] I. Guzmán-Soto, C. McTiernan, M. Gonzalez-Gomez, A. Ross, K. Gupta, E.J. Suuronen, T.-F. Mah, M.
592 Griffith, E.I. Alarcon, Mimicking biofilm formation and development: Recent progress in in vitro and in vivo
593 biofilm models, *iScience* 24 (2021) 102443. <https://doi.org/10.1016/j.isci.2021.102443>.
- 594 [18] Di Shi, G. Mi, M. Wang, T.J. Webster, In vitro and ex vivo systems at the forefront of infection modeling
595 and drug discovery, *Biomaterials* 198 (2019) 228–249. <https://doi.org/10.1016/j.biomaterials.2018.10.030>.
- 596 [19] M.Å. Andersson, L.B. Madsen, A. Schmidtchen, M. Puthia, Development of an Experimental Ex Vivo
597 Wound Model to Evaluate Antimicrobial Efficacy of Topical Formulations, *Int. J. Mol. Sci.* 22 (2021).
598 <https://doi.org/10.3390/ijms22095045>.
- 599 [20] M. Ashrafi, L. Novak-Frazer, M. Bates, M. Baguneid, T. Alonso-Rasgado, G. Xia, R. Rautemaa-
600 Richardson, A. Bayat, Validation of biofilm formation on human skin wound models and demonstration of
601 clinically translatable bacteria-specific volatile signatures, *Sci. Rep.* 8 (2018) 9431.
602 <https://doi.org/10.1038/s41598-018-27504-z>.

- 603 [21] G. Brackman, P. Cos, L. Maes, H.J. Nelis, T. Coenye, Quorum sensing inhibitors increase the
604 susceptibility of bacterial biofilms to antibiotics in vitro and in vivo, *Antimicrob. Agents Chemother.* 55
605 (2011) 2655–2661. <https://doi.org/10.1128/AAC.00045-11>.
- 606 [22] J. Juntke, X. Murgia, N. Günday Türeli, A.E. Türeli, C.R. Thorn, M. Schneider, N. Schneider-Daum, C. de
607 Souza Carvalho-Wodarz, C.-M. Lehr, Testing of aerosolized ciprofloxacin nanocarriers on cystic fibrosis
608 airway cells infected with *P. aeruginosa* biofilms, *Drug Deliv. Transl. Res.* 11 (2021) 1752–1765.
609 <https://doi.org/10.1007/s13346-021-01002-8>.
- 610 [23] J. Wächter, P.K. Vestweber, N. Jung, M. Windbergs, Imitating the microenvironment of native biofilms
611 using nanofibrous scaffolds to emulate chronic wound infections, *J. Mater. Chem. B* 11 (2023) 3212–3225.
612 <https://doi.org/10.1039/d2tb02700c>.
- 613 [24] K. Sebova, M. Bachelor, M. Klausner, P.J. Hayden, J. Oldach, G. Stolper, M. Li, A novel assay for
614 evaluating wound healing in a full-thickness in vitro human skin model, *Toxicology Letters* 238 (2015) S185.
615 <https://doi.org/10.1016/j.toxlet.2015.08.537>.
- 616 [25] L.S. Toni, A.M. Garcia, D.A. Jeffrey, X. Jiang, B.L. Stauffer, S.D. Miyamoto, C.C. Sucharov, Optimization
617 of phenol-chloroform RNA extraction, *MethodsX* 5 (2018) 599–608.
618 <https://doi.org/10.1016/j.mex.2018.05.011>.
- 619 [26] K.J. Livak, T.D. Schmittgen, Analysis of relative gene expression data using real-time quantitative PCR
620 and the 2(-Delta Delta C(T)) Method, *Methods* 25 (2001) 402–408.
621 <https://doi.org/10.1006/meth.2001.1262>.
- 622 [27] S. Tfaili, C. Gobinet, G. Josse, J.-F. Angiboust, M. Manfait, O. Piot, Confocal Raman microspectroscopy
623 for skin characterization: a comparative study between human skin and pig skin, *Analyst* 137 (2012) 3673–
624 3682. <https://doi.org/10.1039/c2an16292j>.
- 625 [28] L. Franzen, M. Windbergs, Applications of Raman spectroscopy in skin research—From skin physiology
626 and diagnosis up to risk assessment and dermal drug delivery, *Adv. Drug Deliv. Rev.* 89 (2015) 91–104.
627 <https://doi.org/10.1016/j.addr.2015.04.002>.
- 628 [29] B.W. Barry, H.G.M. Edwards, A.C. Williams, Fourier transform Raman and infrared vibrational study of
629 human skin: Assignment of spectral bands, *J. Raman Spectrosc.* 23 (1992) 641–645.
630 <https://doi.org/10.1002/jrs.1250231113>.
- 631 [30] M.G. Martinez, A.J. Bullock, S. MacNeil, I.U. Rehman, Characterisation of structural changes in collagen
632 with Raman spectroscopy, *Applied Spectroscopy Reviews* 54 (2019) 509–542.
633 <https://doi.org/10.1080/05704928.2018.1506799>.
- 634 [31] K.J. Livak, T.D. Schmittgen, Analysis of relative gene expression data using real-time quantitative PCR
635 and the 2(-Delta Delta C(T)) Method, *Methods* 25 (2001) 402–408.
636 <https://doi.org/10.1006/meth.2001.1262>.
- 637 [32] H.K.N. Vyas, B. Xia, A. Mai-Prochnow, Clinically relevant in vitro biofilm models: A need to mimic and
638 recapitulate the host environment, *Biofilm* 4 (2022) 100069. <https://doi.org/10.1016/j.biofilm.2022.100069>.
- 639 [33] K. Safferling, T. Sütterlin, K. Westphal, C. Ernst, K. Breuhahn, M. James, D. Jäger, N. Halama, N. Grabe,
640 Wound healing revised: a novel reepithelialization mechanism revealed by in vitro and in silico models, *J.*
641 *Cell Biol.* 203 (2013) 691–709. <https://doi.org/10.1083/jcb.201212020>.
- 642 [34] J. Shepherd, I. Douglas, S. Rimmer, L. Swanson, S. MacNeil, Development of three-dimensional tissue-
643 engineered models of bacterial infected human skin wounds, *Tissue Eng. Part C Methods* 15 (2009) 475–
644 484. <https://doi.org/10.1089/ten.tec.2008.0614>.
- 645 [35] J.F. Cicmanec, I.A. Holder, Growth of *Pseudomonas aeruginosa* in normal and burned skin extract: role
646 of extracellular proteases, *Infect. Immun.* 25 (1979) 477–483. [https://doi.org/10.1128/iai.25.2.477-
647 483.1979](https://doi.org/10.1128/iai.25.2.477-483.1979).
- 648 [36] L.W. Heck, K. Morihara, W.B. McRae, E.J. Miller, Specific cleavage of human type III and IV collagens by
649 *Pseudomonas aeruginosa* elastase, *Infect. Immun.* 51 (1986) 115–118. [https://doi.org/10.1128/iai.51.1.115-
650 118.1986](https://doi.org/10.1128/iai.51.1.115-118.1986).
- 651 [37] R.L. Gallo, K.M. Huttner, Antimicrobial peptides: an emerging concept in cutaneous biology, *J. Invest.*
652 *Dermatol.* 111 (1998) 739–743. <https://doi.org/10.1046/j.1523-1747.1998.00361.x>.
- 653 [38] K.R. Parducho, B. Beadell, T.K. Ybarra, M. Bush, E. Escalera, A.T. Trejos, A. Chieng, M. Mendez, C.
654 Anderson, H. Park, Y. Wang, W. Lu, E. Porter, The Antimicrobial Peptide Human Beta-Defensin 2 Inhibits
655 Biofilm Production of *Pseudomonas aeruginosa* Without Compromising Metabolic Activity, *Front. Immunol.*
656 11 (2020) 805. <https://doi.org/10.3389/fimmu.2020.00805>.

- 657 [39] G. Maisetta, G. Batoni, S. Esin, W. Florio, D. Bottai, F. Favilli, M. Campa, In vitro bactericidal activity of
 658 human beta-defensin 3 against multidrug-resistant nosocomial strains, *Antimicrob. Agents Chemother.* 50
 659 (2006) 806–809. <https://doi.org/10.1128/AAC.50.2.806-809.2006>.
- 660 [40] P. Bulet, R. Stöcklin, L. Menin, Anti-microbial peptides: from invertebrates to vertebrates, *Immunol.*
 661 *Rev.* 198 (2004) 169–184. <https://doi.org/10.1111/j.0105-2896.2004.0124.x>.
- 662 [41] A. Peschel, How do bacteria resist human antimicrobial peptides?, *Trends Microbiol.* 10 (2002) 179–
 663 186. [https://doi.org/10.1016/S0966-842X\(02\)02333-8](https://doi.org/10.1016/S0966-842X(02)02333-8).
- 664 [42] S.L. Percival, J.G. Thomas, D.W. Williams, Biofilms and bacterial imbalances in chronic wounds: anti-
 665 Koch, *Int. Wound J.* 7 (2010) 169–175. <https://doi.org/10.1111/j.1742-481X.2010.00668.x>.
- 666 [43] J. Hurlow, E. Blanz, J.A. Gaddy, Clinical investigation of biofilm in non-healing wounds by high
 667 resolution microscopy techniques, *J. Wound Care* 25 Suppl 9 (2016) S11-22.
 668 <https://doi.org/10.12968/jowc.2016.25.Sup9.S11>.
- 669 [44] K. Kirketerp-Møller, P.Ø. Jensen, M. Fazli, K.G. Madsen, J. Pedersen, C. Moser, T. Tolker-Nielsen, N.
 670 Høiby, M. Givskov, T. Bjarnsholt, Distribution, organization, and ecology of bacteria in chronic wounds, *J.*
 671 *Clin. Microbiol.* 46 (2008) 2717–2722. <https://doi.org/10.1128/JCM.00501-08>.
- 672 [45] G.U. Meduri, S. Kanangat, J. Stefan, E. Tolley, D. Schaberg, Cytokines IL-1beta, IL-6, and TNF-alpha
 673 enhance in vitro growth of bacteria, *Am. J. Respir. Crit. Care Med.* 160 (1999) 961–967.
 674 <https://doi.org/10.1164/ajrccm.160.3.9807080>.
- 675 [46] E. Kaya, L. Grassi, A. Benedetti, G. Maisetta, C. Pileggi, M. Di Luca, G. Batoni, S. Esin, In vitro Interaction
 676 of *Pseudomonas aeruginosa* Biofilms With Human Peripheral Blood Mononuclear Cells, *Front. Cell. Infect.*
 677 *Microbiol.* 10 (2020) 187. <https://doi.org/10.3389/fcimb.2020.00187>.
- 678 [47] C.R. Flach, D.J. Moore, Infrared and Raman imaging spectroscopy of ex vivo skin, *Int. J. Cosmet. Sci.* 35
 679 (2013) 125–135. <https://doi.org/10.1111/ics.12020>.
- 680 [48] L. Franzen, C. Mathes, S. Hansen, M. Windbergs, Advanced chemical imaging and comparison of
 681 human and porcine hair follicles for drug delivery by confocal Raman microscopy, *J. Biomed. Opt.* 18 (2013)
 682 61210. <https://doi.org/10.1117/1.JBO.18.6.061210>.
- 683 [49] S.M. Ali, F. Bonnier, H. Lambkin, K. Flynn, V. McDonagh, C. Healy, T.C. Lee, F.M. Lyng, H.J. Byrne, A
 684 comparison of Raman, FTIR and ATR-FTIR micro spectroscopy for imaging human skin tissue sections, *Anal.*
 685 *Methods* 5 (2013) 2281. <https://doi.org/10.1039/C3AY40185E>.
- 686 [50] A. Gröne, Keratinocytes and cytokines, *Vet. Immunol. Immunopathol.* 88 (2002) 1–12.
 687 [https://doi.org/10.1016/S0165-2427\(02\)00136-8](https://doi.org/10.1016/S0165-2427(02)00136-8).
- 688 [51] M. Andonova, V. Urumova, Immune surveillance mechanisms of the skin against the stealth infection
 689 strategy of *Pseudomonas aeruginosa*-review, *Comp. Immunol. Microbiol. Infect. Dis.* 36 (2013) 433–448.
 690 <https://doi.org/10.1016/j.cimid.2013.03.003>.
- 691 [52] G. Zhao, M.L. Usui, S.I. Lippman, G.A. James, P.S. Stewart, P. Fleckman, J.E. Olerud, Biofilms and
 692 Inflammation in Chronic Wounds, *Adv. Wound Care (New Rochelle)* 2 (2013) 389–399.
 693 <https://doi.org/10.1089/wound.2012.0381>.
- 694 [53] W. Grellner, T. Georg, J. Wilske, Quantitative analysis of proinflammatory cytokines (IL-1beta, IL-6,
 695 TNF-alpha) in human skin wounds, *Forensic Sci. Int.* 113 (2000) 251–264. [https://doi.org/10.1016/S0379-0738\(00\)00218-8](https://doi.org/10.1016/S0379-0738(00)00218-8).
- 697 [54] M. Galle, P. Schotte, M. Haegman, A. Wullaert, H.J. Yang, S. Jin, R. Beyaert, The *Pseudomonas*
 698 *aeruginosa* Type III secretion system plays a dual role in the regulation of caspase-1 mediated IL-1beta
 699 maturation, *J. Cell. Mol. Med.* 12 (2008) 1767–1776. <https://doi.org/10.1111/j.1582-4934.2007.00190.x>.
- 700 [55] Y.-C. Liu, K.-G. Chan, C.-Y. Chang, Modulation of Host Biology by *Pseudomonas aeruginosa* Quorum
 701 Sensing Signal Molecules: Messengers or Traitors, *Front. Microbiol.* 6 (2015) 1226.
 702 <https://doi.org/10.3389/fmicb.2015.01226>.
- 703 [56] J. Marreiro de Sales-Neto, É.A. Lima, L.H.A. Cavalcante-Silva, U. Vasconcelos, S. Rodrigues-
 704 Mascarenhas, Anti-inflammatory potential of pyocyanin in LPS-stimulated murine macrophages,
 705 *Immunopharmacol. Immunotoxicol.* 41 (2019) 102–108. <https://doi.org/10.1080/08923973.2018.1555845>.
- 706 [57] C. Gabay, Interleukin-6 and chronic inflammation, *Arthritis Res. Ther.* 8 Suppl 2 (2006) S3.
 707 <https://doi.org/10.1186/ar1917>.
- 708 [58] B.Z. Johnson, A.W. Stevenson, C.M. Prêle, M.W. Fear, F.M. Wood, The Role of IL-6 in Skin Fibrosis and
 709 Cutaneous Wound Healing, *Biomedicines* 8 (2020). <https://doi.org/10.3390/biomedicines8050101>.

- 710 [59] M. Baggiolini, I. Clark-Lewis, Interleukin-8, a chemotactic and inflammatory cytokine, FEBS Lett. 307
711 (1992) 97–101. [https://doi.org/10.1016/0014-5793\(92\)80909-Z](https://doi.org/10.1016/0014-5793(92)80909-Z).
- 712 [60] C. Schaudinn, C. Dittmann, J. Jurisch, M. Laue, N. Günday-Türelı, U. Blume-Peytavi, A. Vogt, F. Rancan,
713 Development, standardization and testing of a bacterial wound infection model based on ex vivo human
714 skin, PLoS One 12 (2017) e0186946. <https://doi.org/10.1371/journal.pone.0186946>.
- 715 [61] A.V. Nguyen, A.M. Soulika, The Dynamics of the Skin's Immune System, Int. J. Mol. Sci. 20 (2019).
716 <https://doi.org/10.3390/ijms20081811>.
- 717 [62] K.R. Kirker, G.A. James, P. Fleckman, J.E. Olerud, P.S. Stewart, Differential effects of planktonic and
718 biofilm MRSA on human fibroblasts, Wound Repair Regen. 20 (2012) 253–261.
719 <https://doi.org/10.1111/j.1524-475X.2012.00769.x>.
- 720 [63] P.R. Secor, G.A. James, P. Fleckman, J.E. Olerud, K. McInerney, P.S. Stewart, Staphylococcus aureus
721 Biofilm and Planktonic cultures differentially impact gene expression, mapk phosphorylation, and cytokine
722 production in human keratinocytes, BMC Microbiol. 11 (2011) 143. [https://doi.org/10.1186/1471-2180-11-](https://doi.org/10.1186/1471-2180-11-143)
723 [143](https://doi.org/10.1186/1471-2180-11-143).
- 724

Highlights

- All models enable investigation of interactions between biofilms and wound tissue.
- Bacterial quantity and growth pattern strongly depend on wound model viability.
- Label-free Raman spectroscopy revealed changes in tissue composition upon biofilm infection.
- Inflammatory response of infected wound models was consistent with *in vivo* reports.

Journal Pre-proof

Declaration of interests

The authors declare that they have no known competing financial interests or personal relationships that could have appeared to influence the work reported in this paper.

The authors declare the following financial interests/personal relationships which may be considered as potential competing interests:

Maïke Windbergs reports financial support was provided by Stiftung zur Förderung der Erforschung von Ersatz- und Ergänzungsmethoden zur Einschränkung von Tierversuchen. Maïke Windbergs reports financial support was provided by Deutsche Forschungsgemeinschaft. Maïke Windbergs reports financial support was provided by Hessian Ministry for Science and the Arts. Maïke Windbergs reports equipment, drugs, or supplies was provided by Agaplesion Markus Krankenhaus, Frankfurt.
